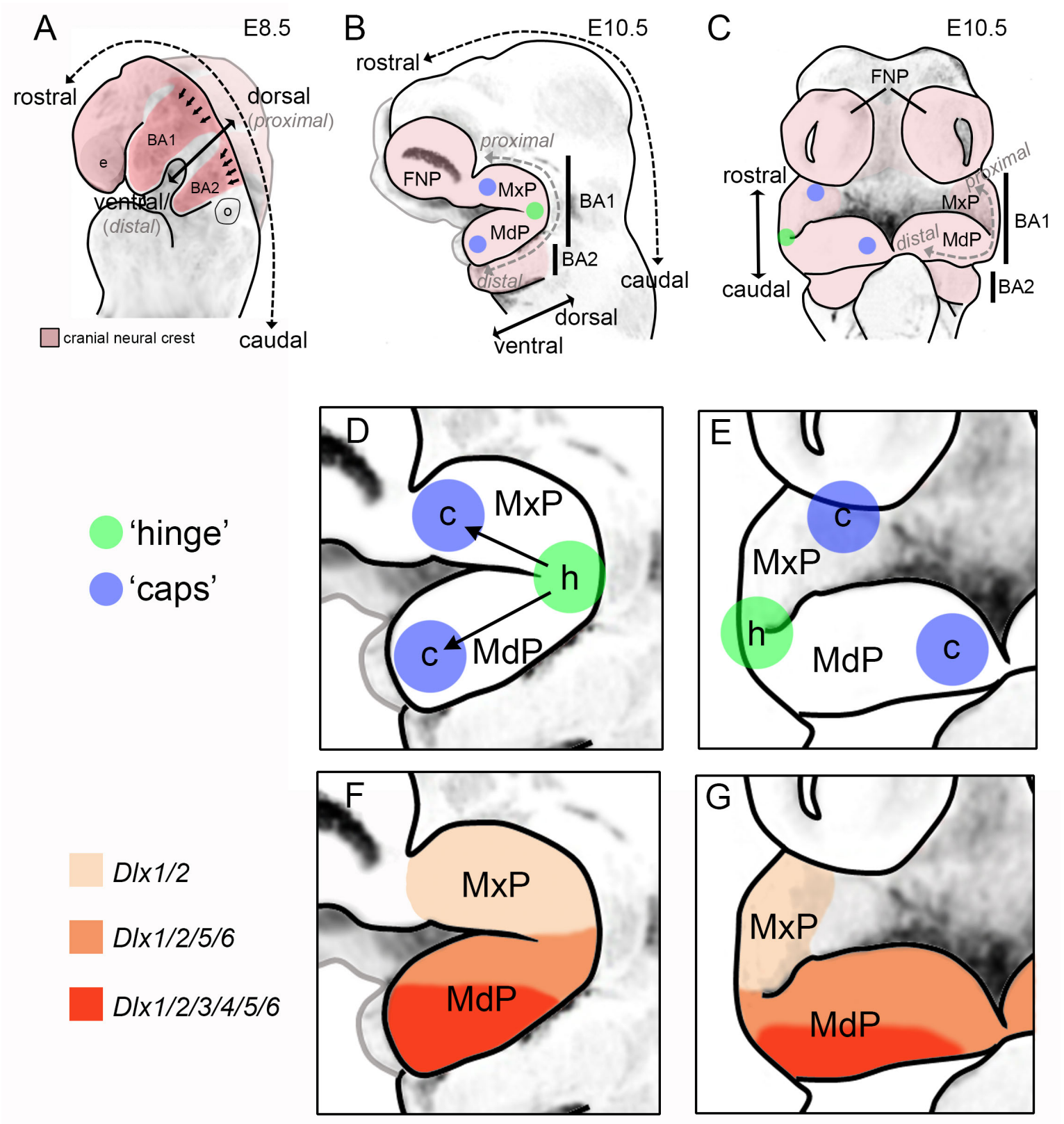
A
E8.5
rostral
dorsal
(proximal)
BA1
e
BA2
ventral/
(distal)
o
cranial neural crest
caudal
B
E10.5
rostral
proximal
FNP
MxP
BA1
MdP
BA2
distal
caudal
dorsal
ventral
C
E10.5
FNP
rostral
proximal
MxP
BA1
distal
MdP
caudal
BA2
'hinge'
'caps'
D
c
MxP
h
c
MdP
E
c
MxP
h
MdP
c
Dlx1/2
Dlx1/2/5/6
Dlx1/2/3/4/5/6
F
MxP
MdP
G
MxP
MdP

Figure S1 – Anatomical locations during mouse craniofacial development. (**A-G**) Dorsolateral (**A**), lateral (**B, D, F**), or ventral (**C, E, G**) schematics of an E8.5 (**A**) or E10.5 (**B-G**) mouse embryo, focusing on craniofacial regions and highlighting key anatomical axes and structures. (**A**) By E8.5, neural crest cells (red shading) that have originated from the dorsal neural tube of hind-, mid-, and forebrain regions are beginning to migrate ventrolaterally into the developing craniofacial structures (note, neural crest cells caudal to branchial arch 2 are not labeled). The dorsal-ventral (proximal-distal) axis of branchial arch 1 is less ambiguous at these earlier developmental stages. (**B, C**) By E10.5, NCCs (pink shading) have ceased migration, and have contributed to the majority of the craniofacial mesenchyme. Additionally, the first branchial arch has become further refined into maxillary (MxP) and mandibular (MdP) prominences – which will form components of the upper and lower jaw, respectively. Note, studies have indicated, at least in avian models, that the MxP may not be derived from NCCs of BA1 (Cerny et al., 2004; Lee et al., 2004). Nevertheless, subdivision of BA1 into these two prominences in mammals somewhat obfuscates anatomical orientations, but traditionally the MxP is referred to as dorsal/proximal and the MdP ventral/distal. BA1 can also be subdivided into the ‘hinge’ (green dot), that is the intersection of the MxP and MdP, and ‘caps’ (blue dots), that is, the regions furthest from the hinge in both the MxP and MdP (Depew and Compagnucci, 2008; Depew et al., 2002; Depew and Simpson, 2006; Depew et al., 2005). We primarily reference these latter terms when discussing BA1. Panels D and E show BA1 and relative positions of the proposed ‘hinge’ and ‘caps’ in more detail, whereas panels F and G highlight the ‘nested Dlx-code’ within the same region. Abbreviations: BA1, branchial arch 1 (i.e. mandibular arch); BA2, branchial arch 2 (i.e. hyoid arch); c, cap; e, eye; FNP, frontonasal prominence; h, hinge; MdP, mandibular prominence; MxP, maxillary prominence; o, otic vesicle.

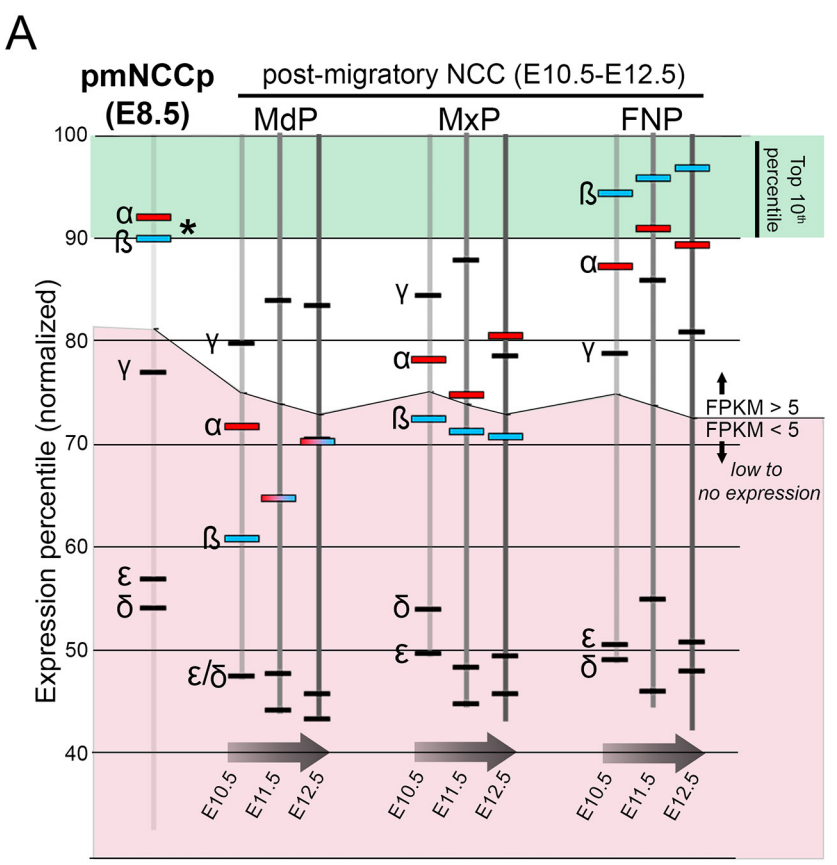

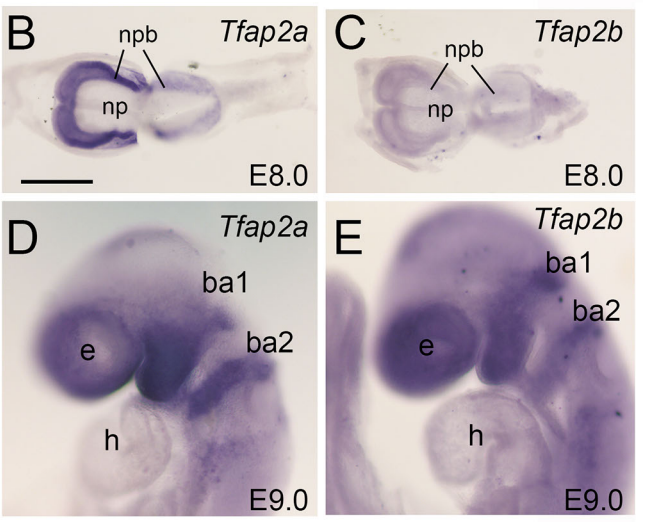

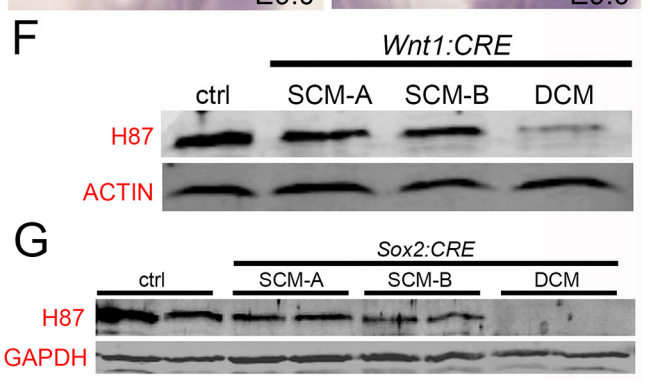

Figure S2 – *Tfap2a* and *Tfap2b* are the most highly expressed paralogs in early mouse cranial NC. (**A**) Chart depicting expression percentile of all genes (based on 'normalized FPKM rank') for E8.5 (Minoux et al., 2017), and E10.5-E12.5 cranial mesenchyme (Hong Li, manuscript in prep, data available at Facebase) – essentially ranking gene expression levels across the entire RNAseq dataset (90-100 on Y-axis, highlighted green, corresponds to the top 10th percentile of expressed genes within a dataset). Ranked position of *Tfap2a* (red bar with label 'α') and *Tfap2b* (blue bar with label 'ß'), as well as other *Tfap2* paralogs (black bars, *Tfap2c* = γ, *Tfap2d* = δ, and *Tfap2e* = ε) are indicated within each dataset. Note, the percentile corresponding to an FPKM of 5 is highlighted in each dataset with genes ranked below this line shown in pink, corresponding to very low or essentially non-expressed genes. (**B-E**) Images of whole-mount *in situ* hybridization of E8.0 dorsal view (**B, C**) or E9.0 lateral view (**D, E**) wild-type embryos, processed with a *Tfap2a* (**B, D**) or *Tfap2b* (**C, E**) antisense riboprobe. (**F**) Collective AP-2α and AP-2ß protein expression levels (as detected by H-87 antibody) in E10.5 facial prominence tissue isolated from the indicated genotypes. ACTIN serves as a loading control. Residual AP-2 immunoreactivity in DCMs represents expression in the ectoderm, which is not targeted by *Wnt1:*CRE. (**G**) Same as in (**F**) with the exception that protein was isolated from E12.5 *Sox2:*CRE embryos of the indicated genotype. GAPDH serves as the loading control. Note, *Sox2:*CRE will target AP-2 expression in both the ectoderm and neural crest derived tissues. Note, for **F** and **G**, each lane corresponds to protein isolated from a single embryo. Abbreviations: ba1, branchial arch 1; ba2, branchial arch 2; FNP, nasal prominence; h, heart; MdP, mandibular prominence; MxP, maxillary prominence; np, neural plate; npb, neural plate border; pmNCCp, premigratory cranial neural crest precursors; Scale bars = 500µM.

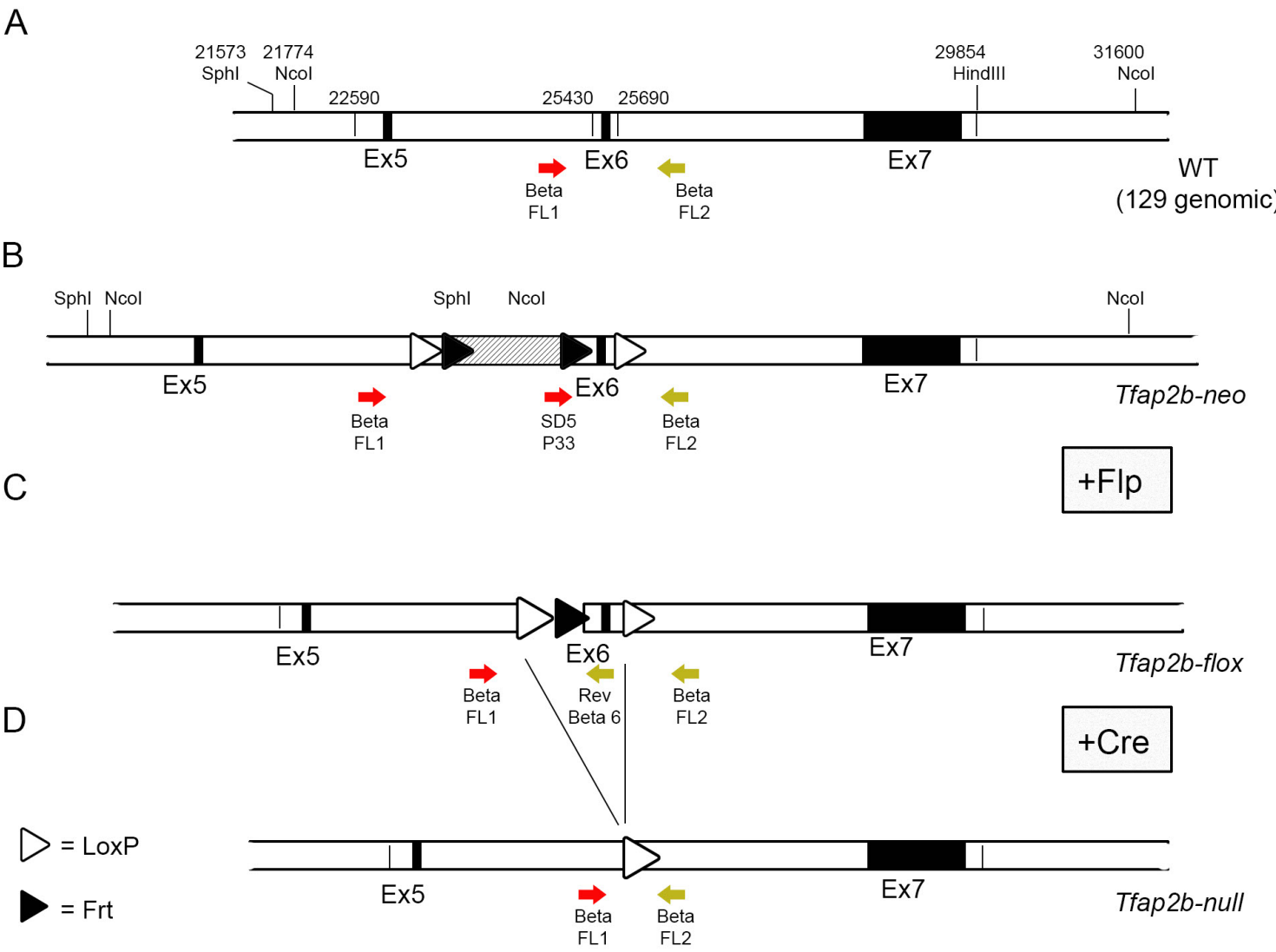

Figure S3 – Schematic of *Tfap2b* alleles generated and utilized in this study. (**A**) Diagram of endogenous *Tfap2b* genomic locus, focused on regions corresponding to exons 5, 6 and 7 (black boxes). Relative genomic positions, including selected restriction sites, are indicated. (**B**) Layout of locus (*Tfap2b-neo*) after targeted homologous recombination, with *neomycin* selection cassette still present (hashed box) and incorporated *LoxP* and *Frt* sites near exon 6. (**C**) Graphic representation of modified *Tfap2b* allele following FLP-mediated recombination resulting in the removal of the *neomycin* cassette and generation of a *Tfap2b* conditional allele (*Tfap2b-flox*). This allele contains *LoxP* recombination sites flanking exon 6 of *Tfap2b*. (**D**) *Tfap2b* locus following CRE-mediated recombination (*Tfap2b*-null). Excision of exon 6 of *Tfap2b* results in a functional null allele in the CRE-recombinase expressing cells/tissues and their derivatives. Colored arrows show positions of primers used for PCR genotyping.

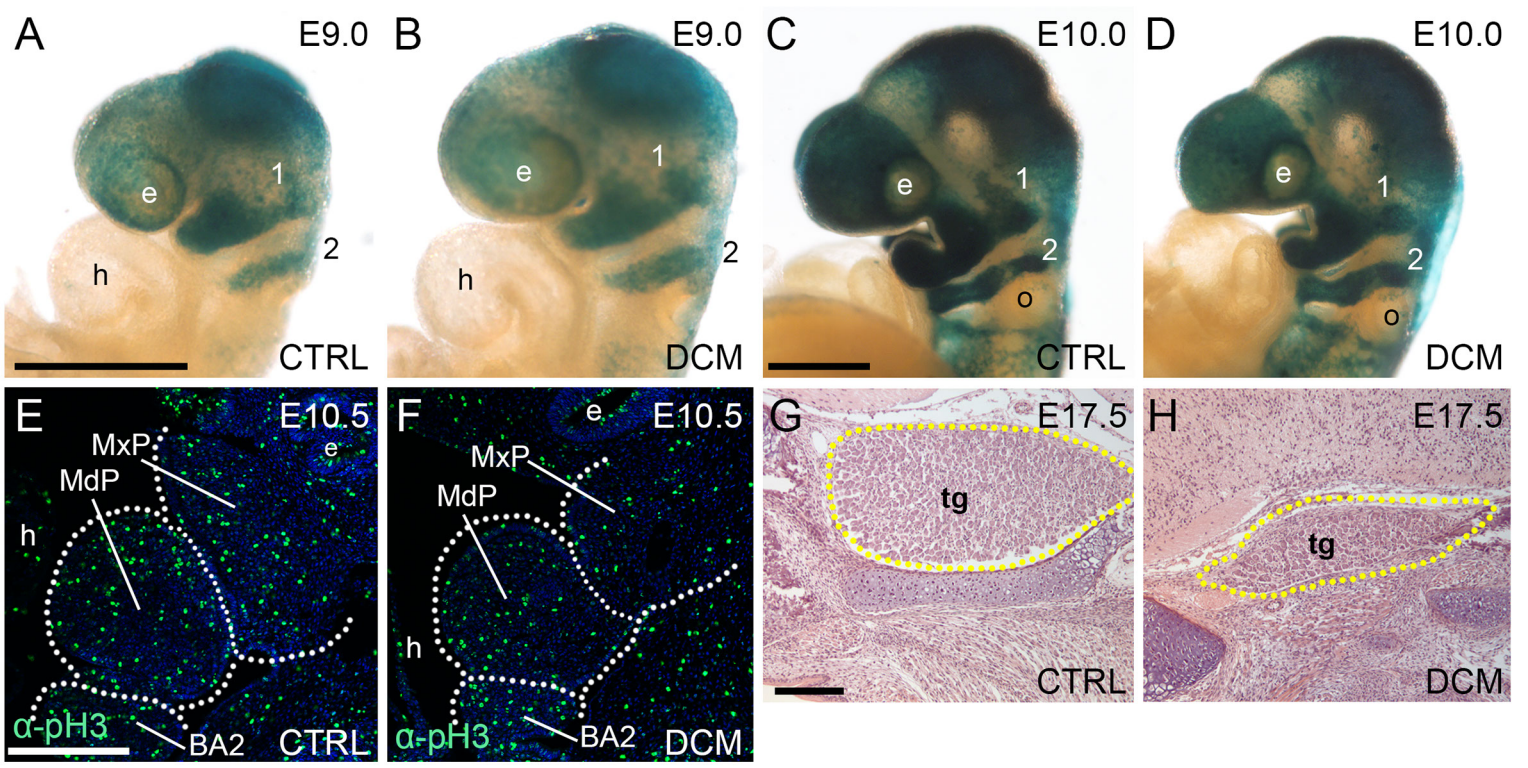

Figure S4 – NC development in *Tfap2a*/*Tfap2b*-*Wnt1*:CRE mutants. (**A-D**) Lateral views of E9.0 (**A, B**) and E10.0 (**C, D**) *Wnt1:*CRE *R26 reporter* embryos, of the indicated genotype processed for ß-galactosidase staining to label NCC lineages. 1 and 2 corresponds to BA1 and BA2 NCC streams, respectively. (**E, F**) Anti-α-phospho-Histone H3 immunofluorescent stained parasagittal paraffin sections through BA1 and BA2 of a control (**E**) or DCM (**F**) E10.5 embryo to label proliferative cells. (**G, H**) H&E stained frontal sections from E17.5 embryos of the indicated genotype, with the trigeminal ganglia outlined by the yellow dashed lines. Abbreviations: BA2, branchial arch 2; e, eye; h, heart; MdP, mandibular prominence; MxP, maxillary prominence; o, otic vesicle; tg, trigeminal ganglion. Scale bars = 500µM.

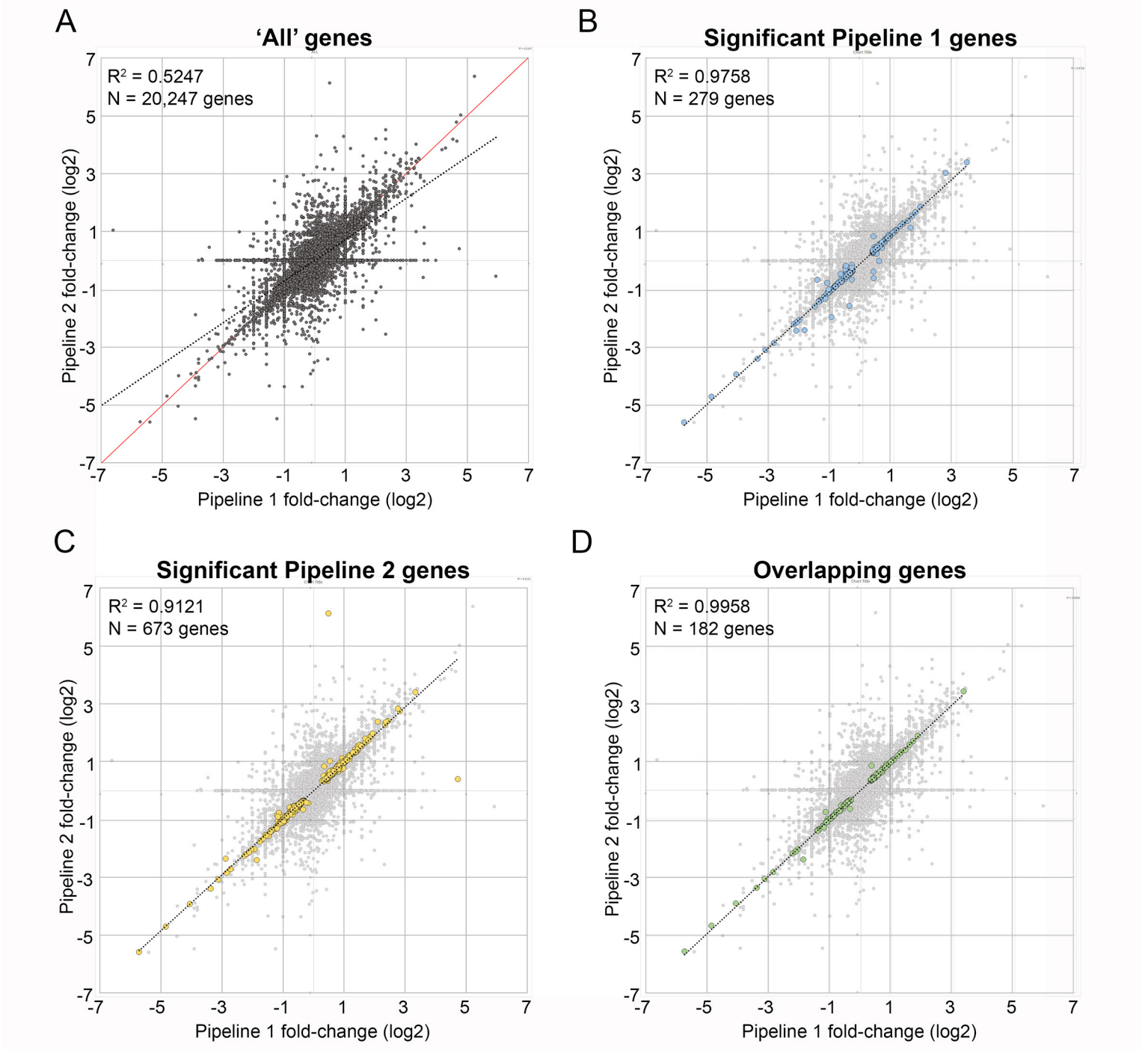

Figure S5 – Comparison of gene expression values between bioinformatic pipelines. (**A-D**) Scatterplots displaying calculated fold-change values (control versus *Tfap2a/Tfap2b-Wnt1*:CRE mutants, log2 scale) between 'Pipeline 1' (X-axis) and 'Pipeline 2' (Y-axis). For **A-D** the calculated R^2-value (correlation coefficient) and number (N) of genes analyzed is reported in the top left corner. For **B-D**, the 'All' gene dataset from panel A is displayed as a light gray graph underneath. **A**) Analysis of all genes. **B**) Analysis of genes only called significant in Pipeline 1 (Class I genes). **C**) Analysis of genes only called significant in Pipeline 2 (Class II genes). **D**) Analysis of overlapping genes between both Class I and II datasets (i.e. Class III genes).

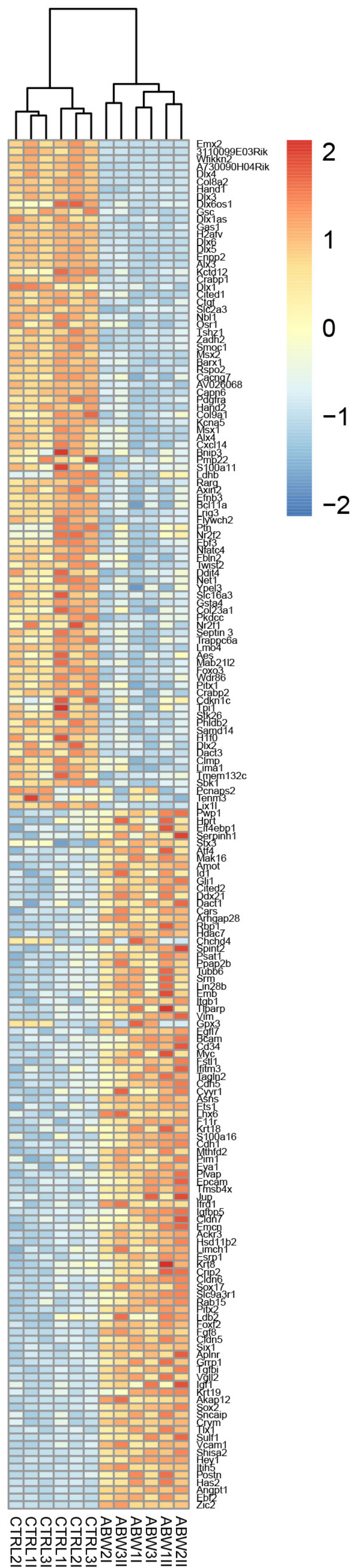

Figure S6 – Detailed hierarchical clustering of 182 ‘high-confidence’ gene-set in *Tfap2a*/*Tfap2b*-*Wnt1*:CRE mutants versus controls. ABW indicates the DCM samples, whereas CTRL are the controls. 1, 2, 3 indicates the biological replicate, and I and II corresponds to data from pipeline 1 or 2, respectively.

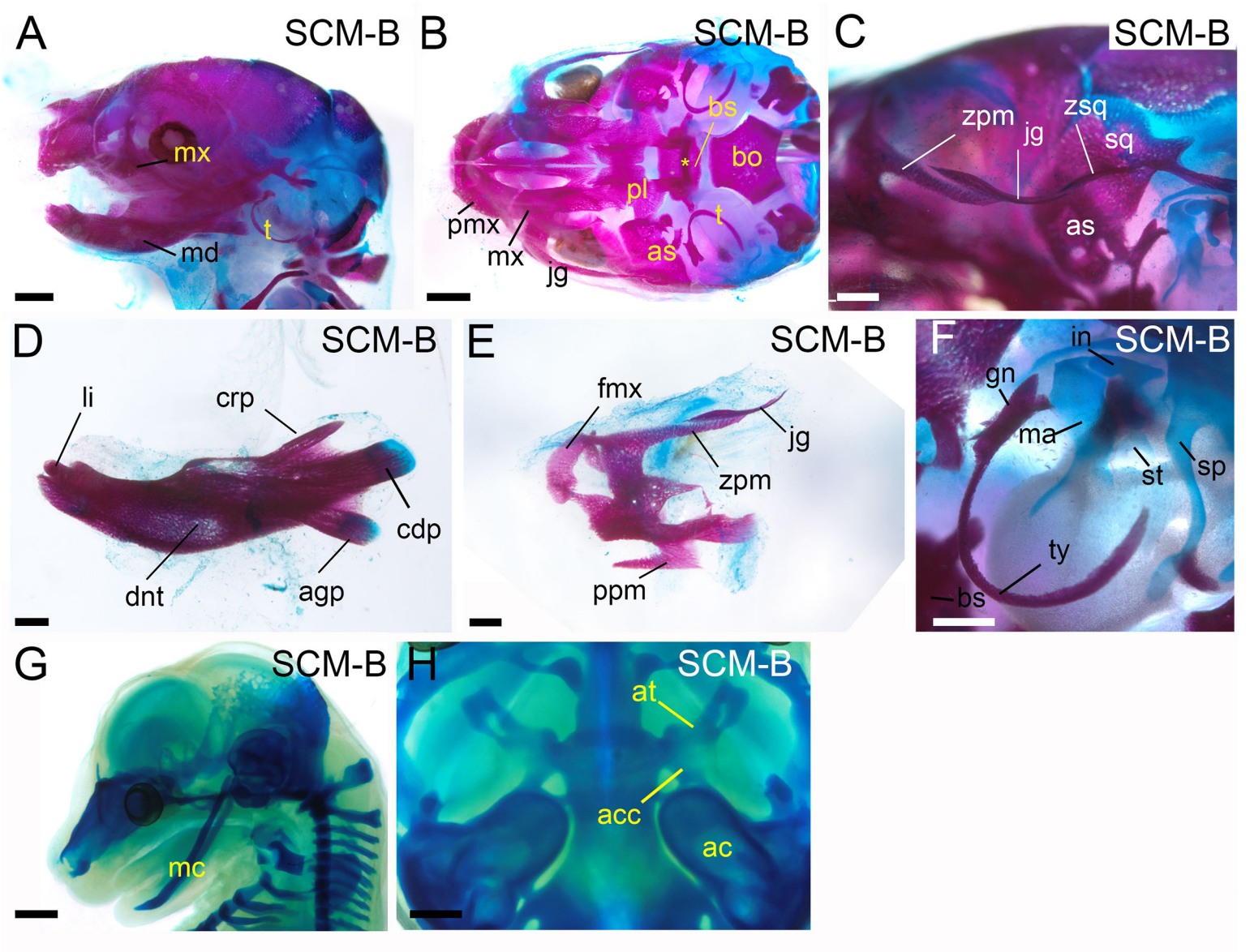

Figure S7 – SCM-B skeletal images. E18.5 skeletal (**A-F**) or E15.5 chondrocranial (**G, H**) preparations. (**A-C**) Whole cranial skeletal preparations in lateral (**A**), ventral (**B**) or ventrolateral (**C**) views, anterior to the left. Note, the mandible has been removed for better visualization in panels B and C, and panel C is a higher magnification image of the zygomatic arch. The asterisk in B highlights the hyoid bone. Mandibular (**D**) or maxillary (**E**) bone shown in isolation, anterior to the left. (**F**) Ventral view, anterior to the upper-left, focusing on the middle ear ossicles. Lateral, anterior left, (**G**) or ventral, anterior up, (**H**) views of the chondrocranium. Compare images to control, SCM-A, and DCM preparations in Figures 5 and 6. Note, SCM-B skeletons resemble controls except for the ~20% that had a cleft secondary palate, and these mutants had palatal process defects typical of this pathology. Abbreviations: ac, auditory capsule; acc, alicochlear commissure; agp, angular process; as, alisphenoid; at, ala temporalis; bo, basioccipital; bs, basisphenoid; cdp, condylar process; crp, coronoid process; dnt, dentary; fmx, frontal process of the maxillary; g, gonial; in, incus; jg, jugal; li, lower incisor; ma, malleus; mc, Meckel's cartilage; md, mandible; mx, maxillary; pl, palatine; pmx, premaxillary; ppm, palatal process of the maxillary; sp, styloid process; sq, squamosal; st, stapes; ty, tympanic; zpm, zygomatic process of the maxillary; zsq, zygomatic process of the squamosal. Scale bars = 1,000 µM (A, B, G), 500µM (C, D, E, F, H).

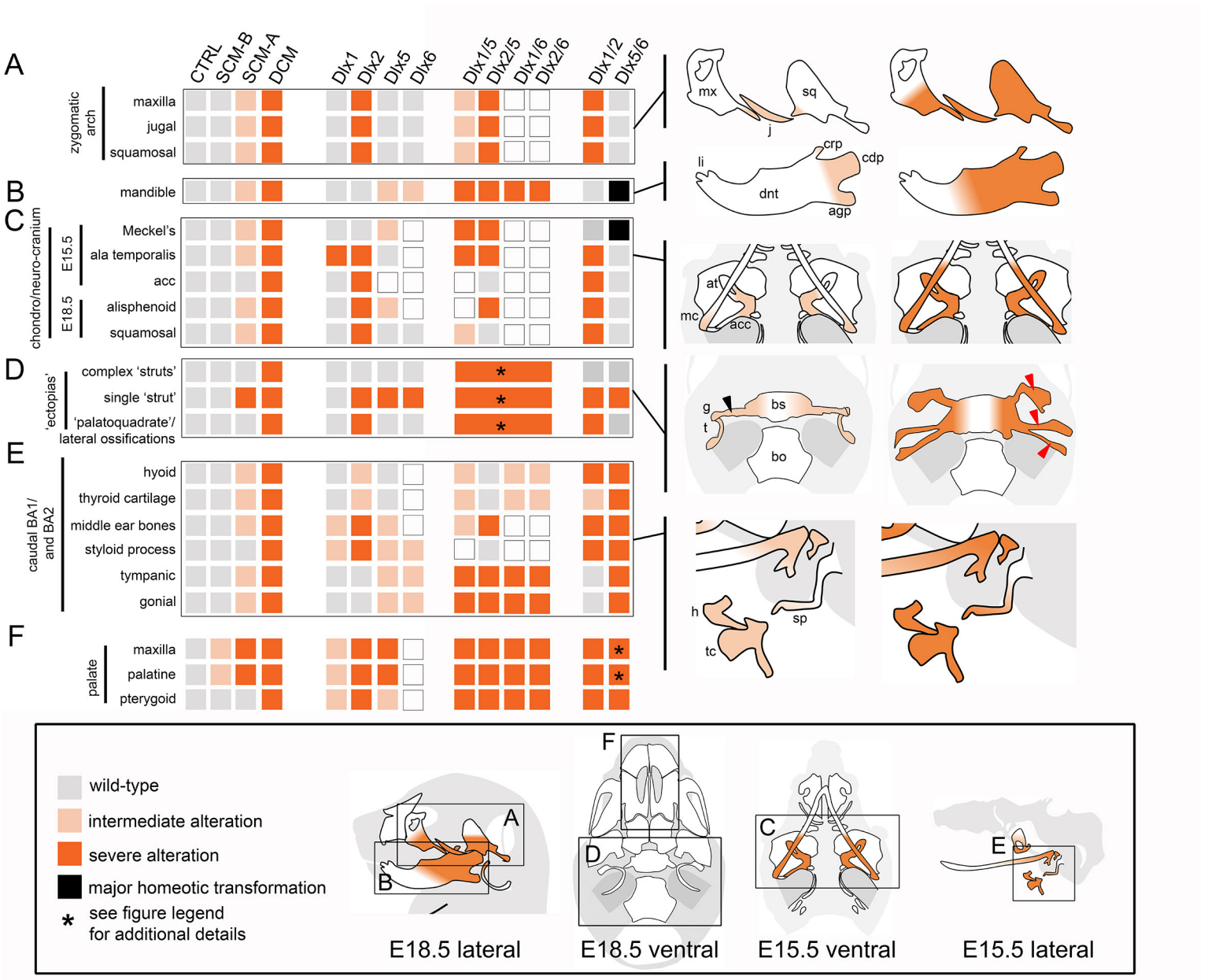

Fig. S8 Summary of overlaps between AP-2α/ß and *Dlx* mutant skeletal phenotypes.

Overview. A heat-map is shown on the left classifying the severity of defects associated with particular components of the craniofacial skeleton at both E15.5 and E18.5 for controls, *Wnt1*:Cre *Tfap2a/b* mutants (based on the images in Figures 5, 6, and S7), and data from the analysis of *Dlx* single and double mutants (1, 2, 5, 6). At the bottom of the figure is shown an overview of the E15.5 and E18.5 skeleton with boxes marking specific regions analyzed in A-F. On the right of the diagram are shown more detailed views of the structures under analysis. These are projected onto a wild-type skeleton, with the exception of the bones of (D) where the first and second columns represent the SCM-A and DCM phenotypes, respectively, and (F) which is not shown. Ectopic struts associated with the cranial base in (D) are shown by arrowheads. In general, grey boxes correspond to relatively wild-type skeletal elements, dark orange boxes represent elements with major developmental defects, whereas light orange represent partial or intermediate defects. Regions where an unshaded box is present represent mouse mutants for which no comment on severity is made. Black boxes indicate major homeotic transformations. Orange color-coding is also used in the schematics to illustrate the severity of the defects. Larger boxes indicate the complexity of *Dlx* allelic combinations that can generate variations of these ectopic skeletal processes. Although several *Dlx* examples are often listed as a reference to the associated defect, such a list is by no means comprehensive. Abbreviations: acc, alicochlear commissure; agp, angular process; at, ala temporalis; bs, basisphenoid; bo, basioccipital; cdp, condylar process; crp, coronoid process; dnt, dentary; g, gonial; h, hyoid; j, jugal; li; lower incisor; mc, Meckel's cartilage; mx, maxillary; sq, squamosal; sp, styloid process; t, tympanic; tc, thyroid cartilage.

(**A**) **Zygomatic arch** (ZGA): Defects in the ZGA range from mild (e.g. loss of the zygomatic process of the squamosal) to severe (more extensive ablations and truncations of the ZGA elements). The appearance of ectopic cartilage/bony elements of unknown lineage (referred to as 'palatoquadrate', discussed more below) are also included in this severe category. For example, SCM-A embryos show a loss of the zygomatic process of the squamosal, similar to [$Dlx1^{-/-};Dlx5^{-/-}$], [$Dlx2^{-/-};Dlx5^{+/-}$], or [$Dlx3^{+/-};Dlx5^{-/-}$] mutants [(Depew et al., 2005), Figure 14E, 13F, and 15F, respectively]. In contrast, DCM embryos display a near ablation of the ZGA (see text),

with an often thickened, truncated zygomatic process of the maxillary bone, as described for example, in *Dlx2*$^{-/-}$*;Dlx5*$^{-/-}$ mutants [(Depew et al., 2005), Figure 11G].

(**B**) **Mandible**: Regions of the mandible most susceptible to loss of AP-2 and Dlx paralogs include the proximal condyles. More mild defects include hypoplastic development of condylar processes, as seen in SCM-A skeletal preparations. Sensitivity of the proximal condyles is also noted in *Dlx5*$^{-/-}$ *and Dlx6*$^{-/-}$ single mutants [(Depew et al., 2005), Figure 7G; (Jeong et al., 2008), Figure 5F, G]. More extreme transformations of the mandible are observed in DCM embryos and are progressively more severe in various *Dlx* allelic combinations [(Jeong et al., 2008), Figure 6G-L; (Depew et al., 2005), Figure 18A-F and Figure 20C, D]. Eventually, in the context of the appropriate *Dlx* paralogs (e.g. *Dlx5*$^{-/-}$*;Dlx6*$^{-/-}$), a threshold is approximated in which the lower-jaw adopts an upper-jaw identity (Beverdam et al., 2002; Depew et al., 2002). Note, such complete transformation is not observed in DCM embryos, although such transformation is often associated with a cleft mandible, which is present in DCM embryos.

(**C**) **Chondro-/Neurocranium**. In respect to the chondrocranial elements, again, intermediate and more severe phenotypes are observed in both AP-2 and *Dlx* mutants. For example, both the upper-jaw ala temporalis and lower-jaw Meckel's cartilage are particularly sensitive to AP-2 and DLX levels. In the context of AP-2 this is observed by mild patterning defects in the ala temporalis of SCM-A embryos and near ablation in DCM embryos. Proximal loss of the ala temporalis was a notable consequence in *Dlx1*$^{-/-}$ [(Qiu et al., 1997), Figure 3B], *Dlx2*$^{-/-}$ [(Qiu et al., 1995), Figure 3B; (Qiu et al., 1997), Figure 2C] and *Dlx1*$^{-/-}$*;Dlx2*$^{-/-}$ [(Qiu et al., 1997), Figure 2D] mutants, with more intermediate defects noted in heterozygous embryos [(Depew et al., 2005), Figure 9F]. Another noted similarly was the loss of the alicochlear commissure in DCM embryos, which was often missing or affected in *Dlx2*$^{-/-}$ [(Qiu et al., 1995), Figure 3B], *Dlx1*$^{-/-}$*;Dlx2*$^{-/-}$ [(Qiu et al., 1997), Figure 2C, D], or more complex compound mutants [e.g. [*Dlx1*$^{+/-}$*;Dlx2*$^{+/-}$*;Dlx3*$^{+/-}$*;Dlx5*$^{+/-}$*;Dlx6*$^{+/-}$], (Depew et al., 2005), Figure 18F]. The lower-jaw, chondrocranial element, Meckel's cartilage, was again intermediately affected in SCM-A embryos (slightly

shorter, with a non-continuous connection with the malleus), whereas in DCM embryos such defects were more severe (see text). Similarly, various *Dlx* mutants display a range of Meckel's cartilage defects. Such defects often impact the proximal end of Meckel's, influencing its association with middle ear structures, such as seen in *Dlx5*$^{-/-}$ mutants [(Depew et al., 2005), Figure 7E). As with the mandible, Meckel's is eventually transformed into its upper-jaw-like counterpart, the ala temporalis in more extreme situations [i.e. *Dlx5*$^{-/-}$*;Dlx6*$^{-/-}$ mutants, (Beverdam et al., 2002; Depew et al., 2002)].

(**D**) **'Ectopias'**: Note, schematics shown in right hand side column 1 and 2 represent ventral views of the cranial base at E18.5 in mutant SCM-A and DCM embryos, respectively. One of the most striking similarities between the AP-2 and Dlx mutants is the appearance of various ectopic structures associated with the cranial base. For example, in SCM-A embryos a single ossified strut (black arrowhead) was observed projecting laterally from the medial basisphenoid, often interacting/fusing with the gonial bone. Several previous reports have identified a highly similar structure in various *Dlx* mutants, including *Dlx2*$^{-/-}$ [(Qiu et al., 1995), Figure 3B, F], *Dlx1*$^{-/-}$*;Dlx2*$^{-/-}$ [(Qiu et al., 1997), Figure 2G, H], *Dlx5*$^{-/-}$ [(Depew et al., 1999), Figure 6D, F, H; (Depew et al., 2005), Figure 19B], *Dlx6*$^{-/-}$ [(Jeong et al., 2008), Figure 6b], and corresponding *Dlx* allelic combinations [e.g. [*Dlx1*$^{-/-}$*;Dlx2*$^{-/-}$*;Dlx5*$^{-/-}$], (Depew et al., 2005), Figure 16B]. More complex ectopic elements (red arrowheads) are noted in DCM embryos, often containing ossified elements with apparent cartilaginous 'joints', a feature again observed in various *Dlx* compound mutants [e.g. *Dlx5*$^{-/-}$*;Dlx6*$^{+/-}$, (Depew et al., 2005), Figure 16C and [*Dlx1*$^{+/-}$*;Dlx2*$^{+/-}$*;Dlx5*$^{-/-}$*;Dlx6*$^{+/-}$] (Depew et al., 2005), Figure 20B]. Also, as briefly mentioned above, loss of the ZGA was often associated with the appearance of ectopic bone and cartilage elements on the lateral side-walls of the cranium, reminiscent of the 'palatoquadrate-like' element discussed in various *Dlx* mutants. Such elements were apparent in DCM embryos, and previously described in, for example, *Dlx2*$^{-/-}$ [(Qiu et al., 1995), 1995, Figure 4B, D], *Dlx1*$^{-/-}$*;Dlx2*$^{-/-}$ [(Qiu et al., 1997), Figure 3E, G], *Dlx2*$^{-/-}$*;Dlx5*$^{-/-}$ [(Depew et al., 2005), Figure 11G], and *Dlx1*$^{-/-}$*;Dlx2*$^{-/-}$*;Dlx5*$^{-/-}$ [(Depew et al.,

2005), Figure 16B] mutants – although variations are noted between genetic models. *Larger boxes indicate the complexity of *Dlx* allelic combinations that can generate variations of these ectopic processes. See references cited for individual details.

(**E**) **Additional BA1 and caudal BA derivatives**: Several other unique features were shared between AP-2 and *Dlx* mutants. In regard to more caudal BA derivatives, the hyoid was often found cleft in SCM-A embryos and fused with the thyroid cartilages. Such features were noted in *Dlx2*$^{-/-}$ [(Depew et al., 2005), Figure 9D], *Dlx1*$^{-/-}$*;Dlx2*$^{-/-}$ [(Depew et al., 2005), Figure 9H], various *Dlx2;Dlx5* compound [(Depew et al., 2005), Figure 11G, I, Figure 12J], *Dlx1*$^{-/-}$*;Dlx2*$^{-/-}$*; Dlx5*$^{-/-}$ [(Depew et al., 2005), Figure 16B], and *Dlx2*$^{-/-}$*Dlx6*$^{-/-}$ [(Jeong et al., 2008), Figure S6L] mutants. More strikingly, the hyoid was fused to the cranial base/pterygoids in DCM embryos. Again, this unusual phenotype was observed in various *Dlx* mutants, notably *Dlx5*$^{-/-}$*;Dlx6*$^{-/-}$ embryos [(Beverdam et al., 2002), Figure 2E]. Additional noted similarities include a variably affected styloid process in SCM-A and DCM embryos, as seen in *Dlx2*$^{-/-}$ [(Qiu et al., 1995), Figure 4B; (Depew et al., 2005), Figure 4E], *Dlx5* $^{-/-}$ [(Acampora et al., 1999), Figure 4B], and *Dlx5*$^{-/-}$*;Dlx6*$^{-/-}$ [(Depew et al., 2002), Figure 3D] mutants. Similarly, the tympanic and gonial bones were variably affected in SCM-A and absent in DCM embryos. Such a continuum was observed in *Dlx* mutants, including hypoplastic formation of these elements in *Dlx6*$^{-/-}$ mutants [(Jeong et al., 2008), Figure 5J], major hypoplasia in *Dlx1*$^{-/-}$*;Dlx6*$^{-/-}$, *Dlx2*$^{-/-}$*;Dlx6*$^{-/-}$ mutants [(Jeong et al., 2008), Figure 6c, d], and complete ablation in *Dlx2*$^{-/-}$*;Dlx5*$^{-/-}$ mutants [(Depew et al., 2005), Figure 11G].

(**F**) **Secondary palatal development**: Although not discussed in detail, several *Dlx* allelic combinations result in clefting of the secondary palate, due to defects in palatal processes of the palatine and maxillary bones – as well as altered pterygoids. Similarly, SCM-A, occasionally SCM-B, and DCM embryos develop overlapping palatal defects.

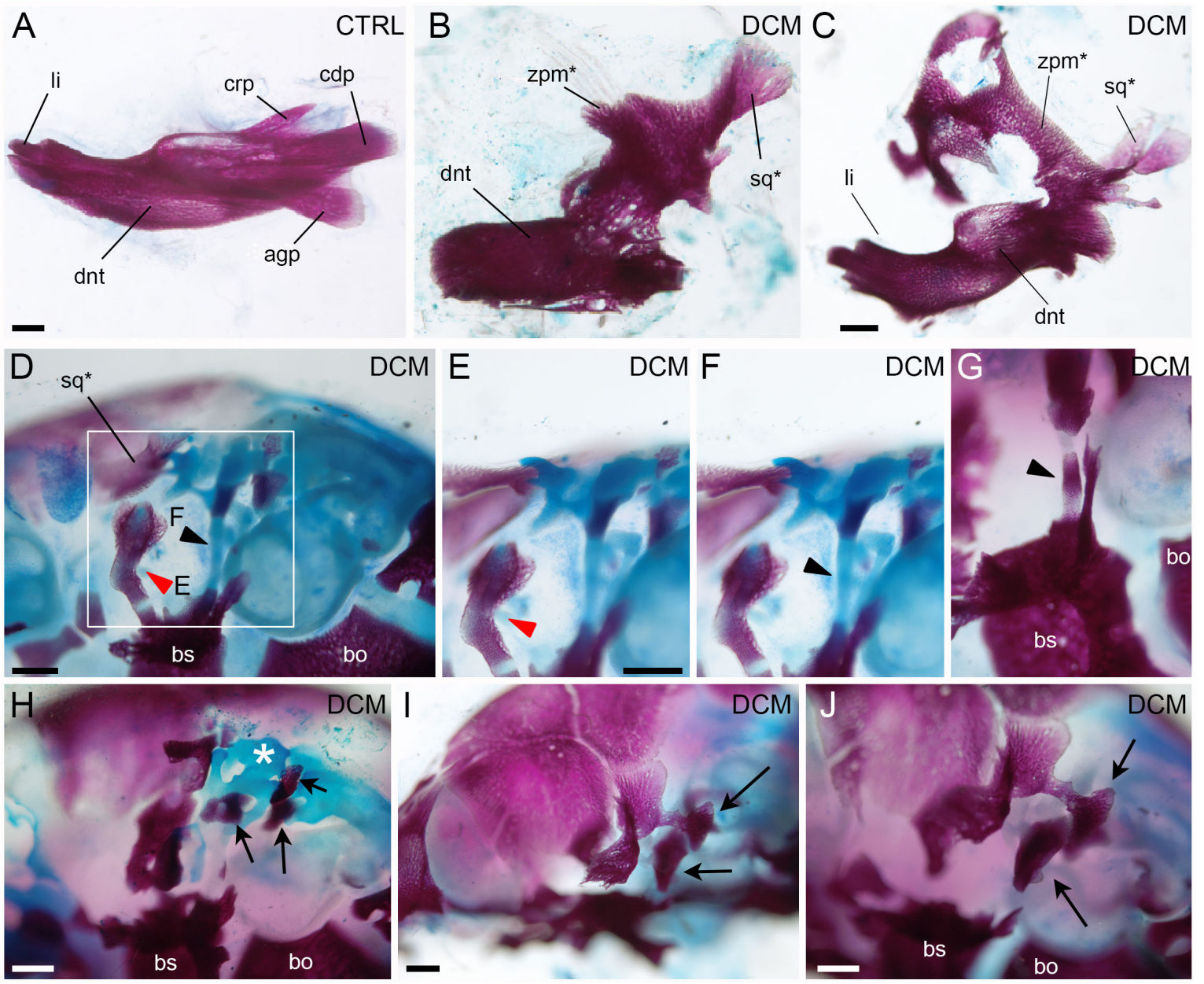

Figure S9 – Additional images of 'Dlx-like' skeletal defects observed in *Tfap2a/Tfap2b-Wnt1*:CRE (DCM) mutants. (**A-J**) Images of E18.5 skeletal preparations of the indicated genotype. (**A-C**) Lateral views (anterior left) of control (**A**) or DCM (**B-C**) mandibles in isolation. Note, the entire maxillary bone is also included in panel **C**, which is fused by its zygomatic process to a modified coronoid process. (**D-J**) Additional ventral views (anterior medial at bottom left) of BA1 hinge-region associated defects detected within the cranial walls and cranial base of DCMs. Various bones (maxillary, palatal, etc) have been removed for better visualization. (**D-G**) highlight ectopic struts (red arrowhead for rostral and black arrowheads for caudal). Panel D is from the same embryo shown in Fig. 6L and panel **E** and **F** are higher magnification images of the boxed area in panel D shot in different focal planes to highlight either the rostral or the caudal strut, respectively. (**H-J**) Show examples of abnormal bone (black arrows) and cartilage elements (white asterisk) with unclear relationship to the normal skeletal derivatives of the cranial base and cranial sidewalls. Comparable control images of the cranial base and side walls are presented in Figs 5 and 6. Abbreviations: agp, angular process; bo, basioccipital; bs, basisphenoid; cdp, condylar process; crp, coronoid process; dnt, dentary; li, lower incisor; sq*, transformed squamosal; zpm* transformed zygomatic process of the maxilla. Scale bars = 500μM.

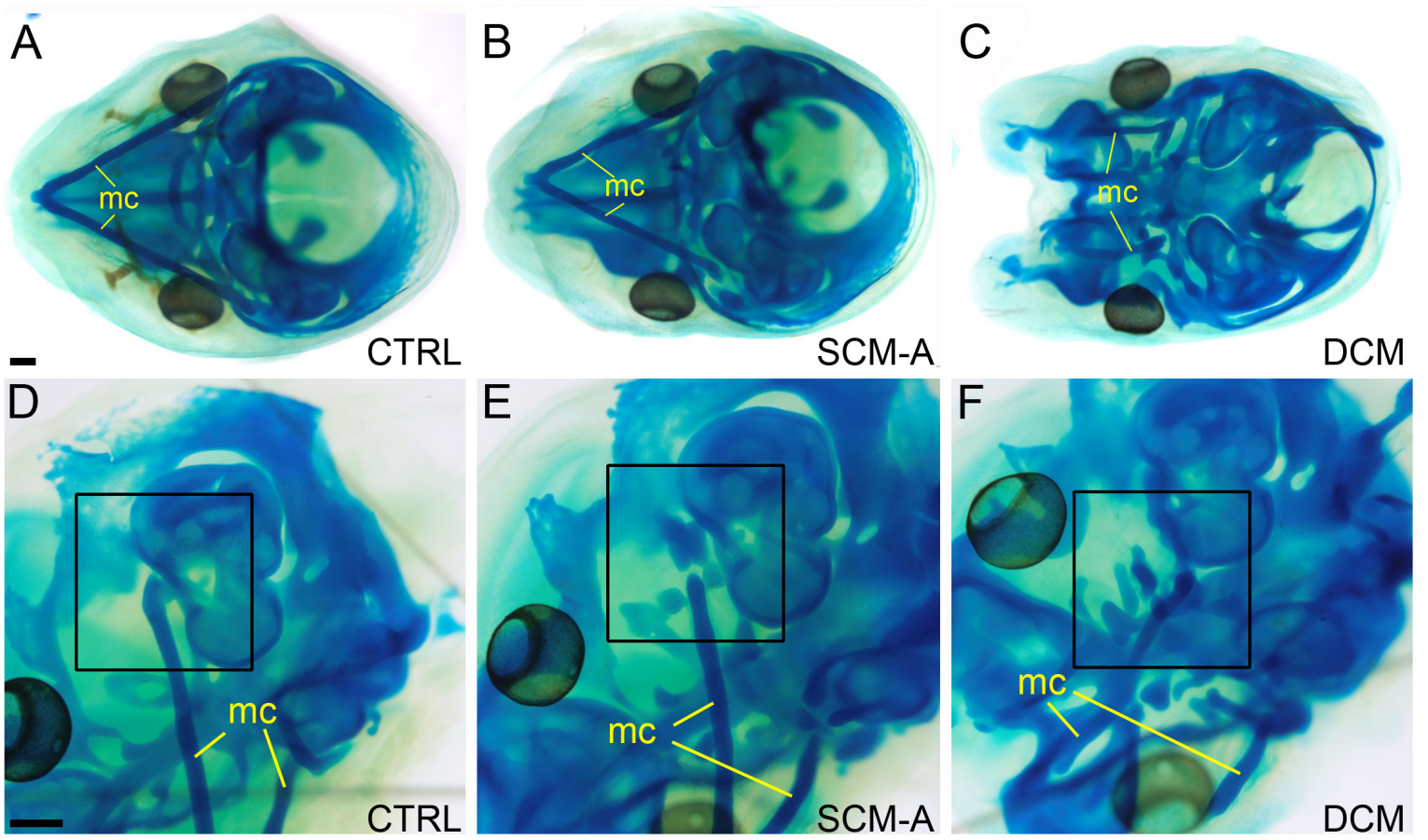

Figure S10 – Additional images of the chondrocranium in *Tfap2a/Tfap2b-Wnt1*:CRE (DCM) and *Tfap2a-Wnt1*:CRE (SCM-A) mutants. (**A-F**) E15.5 cartilage preparations of the indicated genotype shown in either ventral, anterior to the left (**A-C**), or ventrolateral, anterior to the bottom left (**D-F**), views. Boxed regions in D-F highlight the proximal end of Meckel's cartilage. Abbreviations: mc, Meckel's cartilage. Scale bars = 500µM.

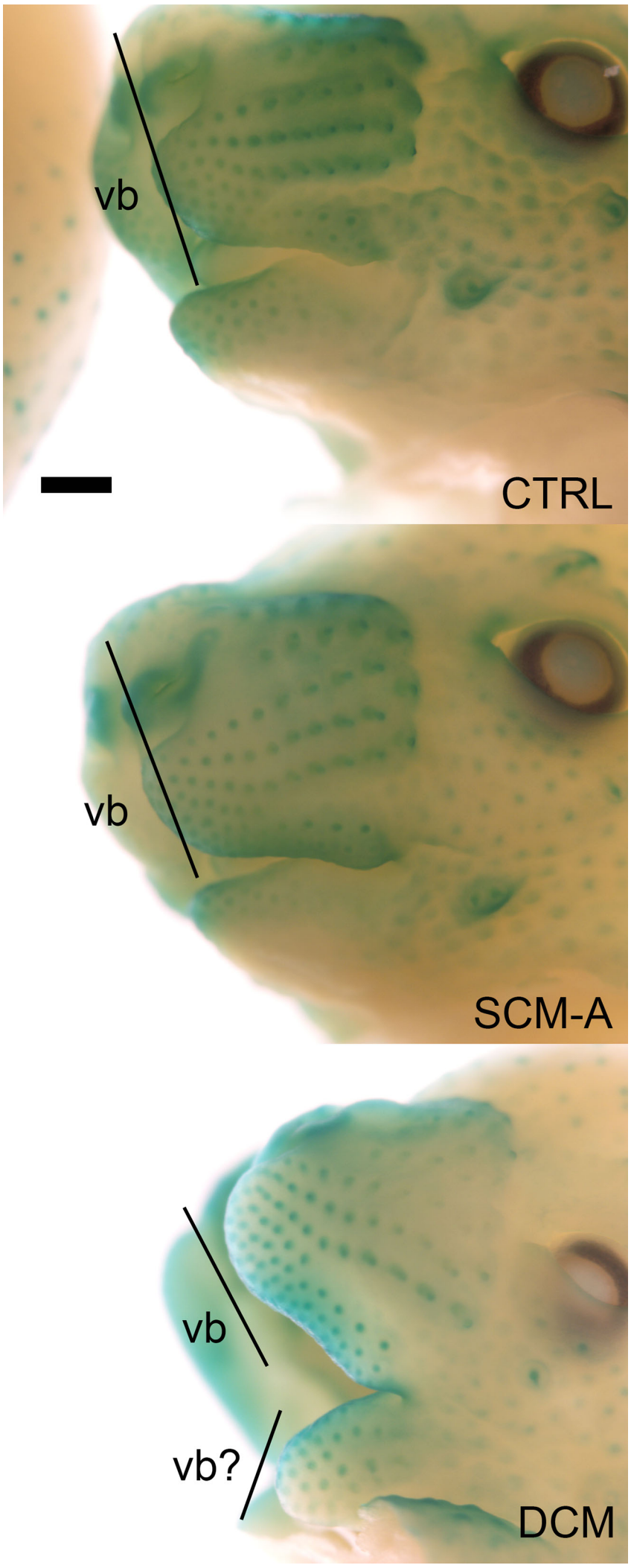
vb
CTRL
vb
SCM-A
vb
vb?
DCM

Figure S11 – Vibrissae-like structures in lower-jaw of *Tfap2a*/*Tfap2b*-*Wnt1*:CRE mutants.

(**A-C**) Lateral views of E14.5 embryos, of the indicated genotype, processed for ß-galactosidase staining. The staining is the result of a *Tfap2a LacZ* knock-in reporter allele (Brewer et al., 2002), highlighting endogenous *Tfap2a* expression – which includes the developing vibrissae (vb). Scale bar = 500µM.

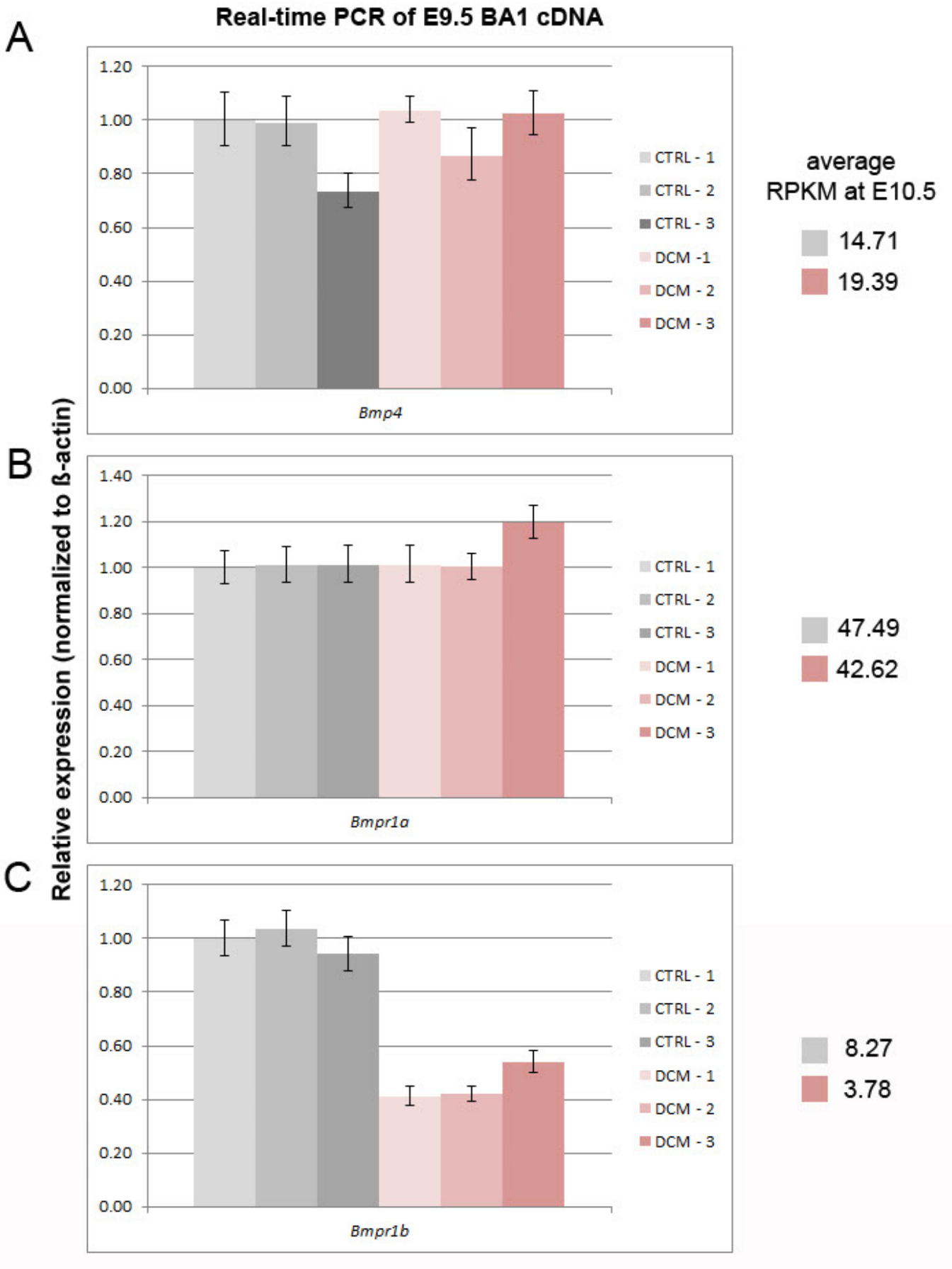

Figure S12. Real-time PCR analysis of BMP-pathway. (**A-C**) Charts summarizing real-time PCR quantification expression levels of *Bmp4* (**A**), *Bmpr1a* (**B**), and *Bmpr1b* (**C**) in E9.5 BA1 cDNA from CTRL and DCM embryos relative to *Actb* (ß-actin). Each bar represents a single embryo, with standard error of technical replicates reported. Values to the right of each chart report the average RPKM value for each gene, based on the E10.5 RNA-seq analysis.

Table S1 – Summary of phenotypes in various AP-2 allelic combinations

Table S1. Genotype and phenotype information for the neural crest *Tfap2a/Tfap2b* gene targeting studies

A. Genotypes derived from mating scheme

Genotype	Description	Abbreviation	CRE
Tfap2a $^{wt/flox}$ *Tfap2b* $^{wt/flox}$	control	ctrl	negative
Tfap2a $^{null/flox}$ *Tfap2b* $^{wt/flox}$	control	ctrl	negative
Tfap2a $^{wt/flox}$ *Tfap2b* $^{null/flox}$	control	ctrl	negative
Tfap2a $^{null/flox}$ *Tfap2b* $^{null/flox}$	control	ctrl	negative
Tfap2a $^{wt/flox}$ *Tfap2b* $^{wt/flox}$ *Wnt1*:CRE	Double conditional heterozygote	DCH	positive
Tfap2a $^{null/flox}$ *Tfap2b* $^{wt/flox}$ *Wnt1*:CRE[ǂ]	Single conditional mutant - *Tfap2a*	SCM-A	positive
Tfap2a $^{wt/flox}$ *Tfap2b* $^{null/flox}$ *Wnt1*:CRE[‡]	Single conditional mutant - *Tfap2b*	SCM-B	positive
Tfap2a $^{null/flox}$ *Tfap2b* $^{null/flox}$ *Wnt1*:CRE*	Double conditional mutant	DCM	positive

[ǂ] ~11% of SCM-A embryos (4 of 38 at E18.5) develop exencephaly, a phenotype that was also noted in ~15% of Tfap2a-Wnt1:CRE mice (Brewer S et al 2004)

[‡] ~22% of SCM-B embryos developed gross cleft secondary palate

* Number of DCM embryos recovered at E18.5, ~4% instead of expected 12.5%, 8 DCMs of 210 total embryos, in comparison to E10.5/E11.5, ~10.5%, 72 DCMs of 695 total embryos, indicates a proportion of embryos die in between these gestational ages. Also, ~50% of embryos (4 of 8 at E18.5) develop exencephaly - for subsequent analysis we concentrated on embryos that lacked exencephaly as this abnormality alone can directly impact craniofacial morphology (Green RM et al 2016)

B. Summary of select craniofacial defects in E18.5 single and double conditional mutant skeletons relative to controls

Genotype (abbreviation)	N	*palate*	*premaxillary*	*mandibular*	*hyoid*	*zygomatic arch*	*squamosal*	*ectopic strut*	*tympanic*
Controls (CTRL)	14	0% (0)	0% (0)	0% (0)	0% (0)	0% (0)	0% (0)	0% (0)	0% (0)
Tfap2a $^{null/flox}$;*Tfap2b* $^{wt/flox}$;*Wnt1CRE (SCM-A)*	18	100% (18)	22% (4)	72%[1] (13)	56%[2] (10)	100%[3] (18)	39%[4] (7)	100%[5] (18)	67%[8] (12)
Tfap2a $^{wt/flox}$;*Tfap2b* $^{null/flox}$;*Wnt1CRE (SCM-B)*	9	22% (2)	0% (0)	0% (0)	0% (0)	0% (0)	0% (0)	0% (0)	0% (0)
Tfap2a $^{null/flox}$;*Tfap2b* $^{null/flox}$;*Wnt1CRE (DCM)*	6	100% (6)	100% (6)	100%[1] (6)	100%[2] (6)	100%[3] (6)	100%[4] (6)	100%[5] (6)	100%[8] (6)

Summary of categories: **palate**, presence of cleft secondary palate; **premaxillary**, presence of midface cleft (split/cleft premaxillary bones, see Figure 5F); **mandibular**, defects found at proximal end of dentary bone (coronoid, condylar, or angular processes); **hyoid**, defects found in hyoid (hypoplastic, 'pinched', cleft); **zygomatic arch** (ZGA), any defects associated with ZGA, including truncated zygomatic processes, missing jugal, etc; **squamosal**, either ectopic foramina in bone and/or hypoplastic/ablated bone; **ectopic strut**, ectopic bony or cartilaginous elements (as described in text); **tympanic**, hypoplastic or missing tympanic bone.

Additional details on phenotypes: [1]Defects in SCM-A skeletons generally corresponded to hypoplastic mandibular processes (see Figure 5N), whereas in DCM skeletons these defects were associated with major loss of the proximal end of the manidble or fusion of lower-jaw to upper-jaw components (see Figure 5O, O'). [2]Defects in SCM-A embryos generally corresponded to small medial 'pinched' or occasional cleft hyoid, with no cranial base fusion (see Figure 6P, S), whereas DCM embryos always had a cleft hyoid found fused to the cranial base (see Figure 6U, X). [3]Defects in SCM-A embryos generally corresponded to shorter zygomatic processes of the maxilla and squamosal (see Figure 5H, K), whereas in DCM embryos these structures were generally ablated (see Figure 5I, L), or more severely truncated (see Figure 5I). [4]A portion of SCM-A skeletons displayed ectopic foramina in the squamosal (see Figure 6H), whereas this structure was either missing or severely malformed in DCM skeletons (see Figure 6I). [5]As described in the text, ectopic struts found in SCM-A and DCM embryos were not identical (compare Figure 6K, L). [8]The tympanic bone, including associated gonial bone, in SCM-A skeletons was hypoplastic (see Figure 6H, K), whereas the bone was completely missing in DCM skeletons (see Figure 6I, L, N).

Table S2 – Class I, Class II, and Class III gene-lists

Click here to Download Table S2

Table S3 – Curated list of genes used for gene set enrichment analysis

Click here to Download Table S3

Table S4 – Information relevant to genotyping primers

ALLELES	PRIMERS	ANNEALING TEMP	PCR PRODUCTS*
Tfap2a-KI (lacZ knock-in)	Alf6/7 (240) : a3KO (200) : iresup (120)	70°C	wt = 500, ki = 300
Tfap2a-null	Alf6/7 (200) : a3KO (240) : Neo3KO (120)	70°C	wt = 500, null = 265
Tfap2a-conditional	Aflox4 : Ascsq	65°C	wt = 496, conditional = 550
Tfap2b-null	Bfl1 : Revbeta6	70°C	wt = 210, conditional = 300‡
Tfap2b-conditional	Bfl1 : Bfl2	70°C	wt = 430, conditional = 550
Wnt1:CRE	Wnt1CRE-F : Wnt1CRE-R	70°C	transgene = ~450
Sox2:CRE	Cre 1 : Cre 3	68°C	transgene = 450
PRIMER SEQUENCES			
Alf6/7	5'-AGG-TGT-AGG-CAG-AAG-TTT-GTC-AGG-GC-3'		
a3KO	5'-CGT-GTG-GCT-GTT-GGG-GTT-GTT-GCT-GAG-GTA-C-3'		
iresup	5'-GCT-AGA-CTA-GTC-TAG-CTA-GAG-CGG-CCC-GGG-3'		
Neo3KO	5'-AAC-GCA-CGG-GTG-TTG-GGT-CGT-TTG-TTC-G-3'		
Aflox4	5'-CCC-AAA-GTG-CCT-GGG-CTG-AAT-TGA-C-3'		
Ascsq	5'-GAA-TCT-AGC-TTG-GAG-GCT-TAT-GTC-3'		
Bfl1	5'-GTC-TGT-TTA-GAA-CAG-CCA-GAG-GCT-GG-3'		
Revbeta6	5'-CCC-GAG-CTA-AGT-GAA-CAG-CTT-CCC-CTG-TAA-GGA-GAG-C-3'		
Bfl2	5'-TCT-GGC-AAG-GCT-CGC-ACT-CAC-AGC-AG-3'		
Wnt1CRE-F	5'-CTC-ATT-GTC-TGT-GGC-CCT-GAC-C-3'		
Wnt1CRE-R	5'-ACG-CCT-GGC-GAT-CCC-TGA-AC-3'		
Cre 1	5'-GCT-GGT-TAG-CAC-CGC-AGG-TGT-AGA-G-3'		
Cre 3	5'-CGC-CAT-CTT-CCA-GCA-GGC-GCA-CC-3'		

*numbers listed for PCR products corresponds to length in basepairs

‡Note, when genotyping *Tfap2b* -null allele, primers were used that did not recognize the deleted allele, but rather indicated if the WT-allele was present (along with generating a conditional-specific PCR product). Embryos in which no WT-allele was present identified those which recieved the paternally derived *Tfap2b* -null allele. This strategy was utilized to prevent false-positives as a result of recombination of the *Tfap2b* -conditional allele.

Numbers in red correspond to the final concentration of primers used, reported in nM. All other primers were used at final concentration of 200nM.

Table S5. Primer sequences

Target	Name	Sequence	Size (bp)	Size+intron*
Six1	Six1-qF	TTAAGAACCGGAGGCAAAGA	154	2191
	Six1-qR	GGGGGTGAGAACTCCTCTTC		
Rspo2	Rspo2-qF	CAGATGCGTTTTTGCCTCTT	158	76547
	Rspo2-qR	CAACCATTGTCCTTCGAACA		
Dlx1	Dlx1-qF	CTACGTCAACTCGGTCAGCA	173	823
	Dlx1-qR	TCTTTTTCCCTTTGCCGTTA		
Dlx2	Dlx2-qF	ATGTCTCCTACTCCGCCAAA	185	600
	Dlx2-qR	GGAGTAGATGGTGCGTGGTT		
Dlx3	Dlx3-qF	CGTTTCCAGAAAGCCCAGTA	168	1678
	Dlx3-qR	ACTGTTGTTGGGGCTGTGTT		
Dlx4	Dlx4-qF	CCATCTCAGCCCTTTCACAG	152	3368
	Dlx4-qR	TGGAGCTGCAGGCTAGAGTAG		
Dlx5	Dlx5-qF	CTGGCCGCTTTACAGAGAAG	220	1257
	Dlx5-qR	CTGGTGACTGTGGCGAGTTA		
Dlx6	Dlx6-qF	ACCATCGCTTTCAGCAGACT	227	1996
	Dlx6-qR	AGAAACGTCCCACACTGGAG		
Bmpr1a	Bmpr1a-qF	GATGATCAGGGAGAAACCACA	162	6526
	Bmpr1a-qR	AACAACAGGGGGCAGTGTAG		
Bmpr1b	Bmpr1b-qF	GCCCATCGAGACTTGAAAAG	176	11272
	Bmpr1b-qR	AAGCTCTCGTCCAGCACTTC		
Bmp4	Bmp4-qF	GGAACCGGGCTTGAGTACC	156	1158
	Bmp4-qR	CACCTCATTCTCTGGGATGC		

*Note, 'Size+intron' corresponds to the predicted genomic size amplified from the primer pair (in basepairs), if the intron is present (i.e., if genomic DNA were present). For all real-time PCR reactions, only the smaller PCR product (Size) was amplified, and absence of the larger product confirmed.